



ELSEVIER

Remote Sensing of Environment 80 (2002) 497–515

Remote Sensing  
of  
Environment

www.elsevier.com/locate/rse

## Preliminary estimate of calibration of the moderate resolution imaging spectroradiometer thermal infrared data using Lake Titicaca

Zhengming Wan<sup>a,\*</sup>, Yulin Zhang<sup>a</sup>, Zhao-liang Li<sup>a,1</sup>, Ruibo Wang<sup>a</sup>, Vincent V. Salomonson<sup>b</sup>,  
Arnaud Yves<sup>c</sup>, Roland Bosseno<sup>c</sup>, Jean Francois Hanocq<sup>d</sup>

<sup>a</sup>*Institution for Computational Earth System Science, University of California, Santa Barbara, CA 93106, USA*

<sup>b</sup>*Earth Sciences Directorate, Goddard Space Flight Center, Greenbelt, MD 20771, USA*

<sup>c</sup>*French Institute of Research and Development, La Paz, Bolivia*

<sup>d</sup>*INRA Bioclimatology, Avignon Cedex, France*

Received 26 February 2001; received in revised form 8 October 2001; accepted 10 October 2001

### Abstract

The absolute radiometric accuracy of Moderate Resolution Imaging Spectroradiometer (MODIS) thermal infrared (TIR) data was evaluated with in situ data collected in a vicarious calibration field campaign conducted in Lake Titicaca, Bolivia during May 26 and June 17, 2000. The comparison between MODIS TIR data produced by the version 2.5.4 Level-1B code and the band radiances calculated with atmospheric radiative transfer code MODTRAN4.0 based on lake surface kinetic temperatures measured by five IR radiometers deployed in the high-elevation Lake Titicaca and the atmospheric temperature and water vapor profiles measured by radiosondes launched on the lake shore on June, 15 2000, a calm clear-sky day, shows good agreements in bands 31 and 32 (within an accuracy of 0.4%) in the daytime overpass case. Sensitivity analysis indicates that the changes on the measured atmospheric temperature and water vapor profiles result in negligible or small effects on the calculated radiances in the atmospheric window bands (bands 20–23, 29, and 31–32). Therefore, comparisons for these bands were made for cases when lake surface temperature measurements were available but no radiosonde data were available and in subareas of  $10 \times 16$  pixels where there was no in situ measurement but MODIS brightness temperatures in band 31 vary within  $\pm 0.15$  K by using the validated band 31 to determine lake surface temperatures through the MODTRAN4.0 code. Comparisons and error analysis show that the specified absolute radiometric accuracies are reached or nearly reached in MODIS bands 21, 29, and 31–33 and that there is a calibration bias of 2–3% in bands 20, 22, and 23. The error analysis also shows that the radiosondes cannot provide accurate atmospheric temperature and water vapor profiles to estimate the calibration accuracies in the atmospheric sounding bands (bands 24–25, 27–28, and 34–36) at the specified 1% level and that the calibration accuracy in the ozone band 30 cannot be estimated without in situ measurements of ozone. © 2002 Elsevier Science Inc. All rights reserved.

### 1. Introduction

The Moderate Resolution Imaging Spectroradiometer (MODIS) was developed as the keystone instrument (Salomonson, Barnes, Maymon, Montgomery, & Ostrow, 1989) on the Earth Observing System (EOS) AM-1 (also named Terra) and EOS PM (named Aqua) platforms (King, Herring, & Diner, 1995) for global studies of atmosphere, land, and ocean processes (Esaias et al., 1998; Justice et al., 1998;

King, Kaufman, Menzel, & Tanré, 1992). The MODIS instrument scans  $\pm 55^\circ$  from nadir in 36 bands, with bands 1–19 and 26 in the visible and near infrared (IR) range and the remaining bands in the thermal IR (TIR) from 3 to 15  $\mu\text{m}$ . Barnes, Pagano, and Salomonson (1998) described the prelaunch characteristics of the MODIS Proto-Flight Model (PFM) flown on Terra, including the relative spectral response (RSR) functions and calibration. The specification of noise equivalent temperature difference (NEDT) for MODIS bands are given in Table 1. The MODIS TIR bands are calibrated through the full-aperture onboard blackbody (BB) and space views. The effective emissivity of the BB is better than 0.992, and BB temperature measurements are made via 12 evenly spaced precision thermometers. The scan mirror views the BB and space during each scan line,

Corresponding author. Tel.: +1-805-893-4541; fax: +1-805-893-2578.

E-mail address: wan@icess.ucsb.edu (Z. Wan).

<sup>1</sup> On temporary leave from GRTR/LSIIT/ENSPS, Parc d'Innovation, 5 Bd. Sebastien Brant, 67400 Illkirch-Graffenstaden, France.

Table 1

Specifications of the EOS MODIS bands and the TIR band NEDT values (in column 9) estimated from early MODIS data (Wan, 2002)

Band	IFOV	Primary use <sup>a</sup>	Band	Bandwidth ( $\mu\text{m}$ )	NEDT specified (K)	NEDT estimated (Wan, 2002)	Primary use <sup>a</sup>
	620–670	250 m	L	20	3.660–3.840	0.05	O, L
2	841–876	250 m	A, L	21	–3.989	2.00	fire, volcano
3	459–479	500 m	L	22	–3.989	0.07	A, L
4	545–565	500 m	L	23	–4.080	0.07	A, L
	1230–1250	500 m	L	24	–4.498	0.25	A
	1628–1652	500 m	A, L	25	–4.549	0.25	A
	2105–2155	500 m	A, L	27	–6.895	0.25	A
	405–420	1 km	O	28	–7.475	0.25	A
9	438–448	1 km	O	29	–8.700	0.05	L
10	483–493	1 km	O	30	–9.880	0.25	ozone
11	526–536	1 km	O	31	–11.280	0.05	A, L
12	546–556	1 km	O	32	–12.270	0.05	A, L
13	662–672	1 km	O	33	–13.485	0.25	A, L
14	673–683	1 km	O	34	–13.785	0.25	A
15	743–753	1 km	A	35	–14.085	0.25	
16	862–877	1 km	A	36	–14.385	0.35	A
17	890–920	1 km	A				
18	931–941	1 km	A				
19	915–965	1 km	A				
26	1360–1390	1 km	cirrus				

enabling a two-point radiometric calibration of the 16 thermal bands every 1.477 s (Barnes et al., 1998). The specification of absolute radiometric accuracy for MODIS TIR bands is  $\pm 1\%$  for all bands, except 0.75% for band 20, 10% for band 21, and 0.5% for bands 31 and 32 (Guenther et al., 1998). The Earth scenes are sampled 1354 times over the range of principle scan angles from  $-55$  to  $55^\circ$  in 1KM bands, which are composed of 10 channels (individual detector elements) in each band. The MODIS level-1B data product is broken into granules approximately 5-min long each and stored in hierarchical data format (HDF). The MODIS level-1B 1KM Earth view science data set (SDS) for the TIR bands, EV\_1KM\_Emissive, is stored as 15-bit unsigned integers, with the high-order bit of the 16-bit word set to 1. Associated with each SDS value is uncertainty information about that value. The information is reported in EV\_1KM\_Emissive\_Uncert\_Indexes as an 8-bit word, with the four most significant bits used for an uncertainty index and the other four bits used for a scene contrast index. More details are available at the MODIS Calibration Support Team (MCST) homepage [mcstweb.gsfc.nasa.gov/Home.html](http://mcstweb.gsfc.nasa.gov/Home.html), where there are listed areas of known concerns with the MODIS level-1B TIR data including incomplete knowledge of sensor response across scan (RVS), optical cross-talk from band 31 to 32–36, and electronic cross-talk amongst bands 5–7 and 20–26.

The MODIS was successfully launched from Vandenberg Air Force Base, California on December 18, 1999. The MODIS first light, early engineering image over the Gulf of Mexico and Eastern North America was acquired on February 24, 2000. The MODIS calibrated radiance, daily level-1B data product (MOD02), and geolocation product (MOD03)

are available to the public at the EOS Data Gateway (<http://redhook.gsfc.nasa.gov/~imswww/pub/imswelcome>).

According to a recent study (Wan, in press) of the channel-dependent noise and systematic error in MODIS TIR channel data, using early MODIS data acquired over lake and ocean sites in clear-sky days, in 14 cases of subarea sites with a size of 10 lines by 16 pixels each line, where the brightness temperature in band 31 changes within  $\pm 0.1$  K, the NEDT specification is reached in all channels of the 16 MODIS TIR bands except three noisy channels (corresponding to the ninth detector in bands 21 and 24 and the fourth detector in band 22). Therefore, it is possible and necessary to evaluate the radiometric accuracy with real MODIS TIR data. It is important to evaluate the absolute radiometric calibration accuracy of the MODIS TIR data in its normal operations in orbit so that it is possible to assess the effects of uncertainties in the calibration accuracy on the MODIS products that depend on the MODIS TIR data, such as land surface temperature (LST; Wan & Dozier, 1996; Wan & Li 1997), sea surface temperature (SST), and atmospheric temperature and water vapor profiles. Because the difference between brightness temperatures in bands 31 and 32 is used in split-window algorithms to correct the atmospheric effects in order to retrieve SST and LST values, any error in the temperature difference will be amplified (because it is multiplied by a coefficient much larger than one in these algorithms) and propagated into the SST and LST products. Therefore, the SST and LST algorithms need a tight requirement for the relative calibration accuracy between bands 31 and 32, i.e., accuracy of the difference between brightness temperatures in these two bands.

In the following sections, we will discuss why Lake Titicaca is used as a vicarious calibration site. Then, we will present an approach to the quantitative estimation of the calibration of MODIS TIR data with in-depth discussion on some technical issues related to this approach. Lastly, results of in situ measurement data and atmospheric radiative transfer simulations and comparison to real MODIS data will be presented along with error analysis leading to some final conclusions.

## 2. The use of Lake Titicaca as a vicarious calibration site

According to the experience gained in our field campaigns for the validation of the MODIS and the MODIS Airborne Simulator (MAS) LST algorithms and products (Snyder, Wan, Zhang & Feng, 1997; Wan & Dozier, 1996; Wan & Li 1997; Wan et al., 1999), the major sources of uncertainties in the validation of TIR products include the uncertainties in atmospheric temperature and water vapor profiles and the spatial variations in surface temperature and emissivity within the TIR scene.

The radiosonde measurement usually takes more than 1 h to acquire a set of atmospheric temperature and water vapor profiles. During this time, the radiosonde balloon may shift 20–50 km in the horizontal direction in windy conditions. Considering the high temporal and spatial variations in the atmospheric status (especially water vapor) and the errors in radiosonde data, the differences between the measured temperature and water vapor profiles and the actual profiles for the real satellite observation may be quite large. Padilla, Leyva, and Mosino (1993) made psychrometric measurements for study of atmospheric humidity behavior at two places in Mexico, one in the Chaultepec Heights in the western zone of Mexico City at 2300-m MSL and another in Rancho Viejo, a mountainous wooded area at 2700-m MSL. The distance between these places is approximately 68 km. They found that the mixing ratio mean values for clear-sky days in the 1989 rainy season vary 30% in the period of 09:00–12:00 h local time and 40% in 12:00–15:00 h. Bruegge et al. (1992) reported that water vapor column abundances retrieved from the Airborne Visible IR Imaging Spectrometer (AVIRIS) data during the First ISLSCP Field Experiment (FIFE) over the Konza Prairie, KS on August 31, 1990 indicated that the spatial variability over scales associated with surface topography and the underlying vegetation may be greater than 10%. Therefore, the accuracy and representativeness of measured atmospheric profiles are crucial for the success of vicarious calibration activities.

It is easy to rationalize the use of clear-sky oceans or lakes as the validation sites for the absolute calibration of TIR radiance because the flat water surface (under low wind conditions) provides the only Earth scene in which emissivity and its polarization can be accurately calculated (Born & Wolfe, 1980) from the refractive index of water

(Hale & Query, 1973). For example, the performance of the MAS has been validated in field campaigns conducted in the Gulf of Mexico (King et al., 1996) and Mono Lake (Wan et al., 1999). Although the emissivities of snow and ice are comparable to water emissivity in the TIR range of interest, they, however, change with particle size, surface roughness, and the presence of meltwater so that it is difficult to know the exact values of the spectral emissivities of snow and ice in the field to the accuracy required for the validation of MODIS absolute radiance in the TIR region.

Smith et al. (1996) showed that the SST was measured to an accuracy believed to be better than 0.1 °C with the Atmospheric Emitted Radiance Interferometer (AERI) over the Gulf of Mexico during a 5-day oceanographic cruise in January 1995. They also showed an advantage of microwindows (the narrow windows between absorption lines), where the atmospheric effects are small when observed with high-spectral resolution instruments such as High-Resolution Interferometer Sounder (HIS) on the NASA ER-2. In these microwindows, the uncertainty in the calculated top of the atmosphere (TOA) radiances based on measured atmospheric temperature and water vapor profile is weakly dependent on the accuracy of the atmospheric temperature and water vapor profile. However, for other narrow bands of HIS and for moderate-resolution TIR channels of MODIS, this uncertainty may be strongly dependent on the accuracy of the atmospheric temperature and water vapor profile and on the accuracy of the empirical water vapor continuum absorption (Clough, Kneizys, Shettle, & Anderson, 1986) used in atmospheric radiative transfer calculations. Another consideration is the spatial variation in SST, which is often larger than 0.1 °C.

Lake Titicaca is a very good validation site for the TIR absolute radiances because of the following reasons: (a) it is a high-elevation (3841 m above sea level) lake located in a large plateau; (b) it has a large size of open water surface (8100 km<sup>2</sup>); (c) there are only very light boating activities on the lake in the winter; (d) the spatial variation in the lake surface temperature is often very small so that the maximum difference in brightness temperatures of MODIS band 31 in a subarea larger than 30 × 30 km is not larger than 0.5 K, for example, in the MODIS data on May 24 and June 3, 15, 21, and 23, 2000; (e) over the lake area and its surroundings, the atmosphere is dry in the winter; and (f) there is a high chance of clear-sky days in the winter and high visibilities (low aerosol densities) in clear-sky days. Therefore, the effects of the uncertainties in atmospheric conditions, aerosol distribution, and the empirical water vapor continuum absorption on the satellite TIR data will be smaller over Lake Titicaca.

Fig. 1 is a map of Lake Titicaca. The west side is in Peru and its east side is in Bolivia. Fig. 2 is a MODIS color composite image over Bolivia on June 15, 2000, with brightness temperatures in bands 20, 29, and 31 as RGB (red, green, and blue) components. The uniformly gray area



Fig. 1. A map of Lake Titicaca and the location of Village Huatajata, which was the base for our vicarious calibration field campaign in May–June 2000.

in the middle is Lake Titicaca. Fig. 3 is a color photo taken on 15 June 2000 during field campaign in east Lake Titicaca.

### 3. Approach

We use the following approach to evaluate the absolute calibration accuracy of MODIS TIR data with in situ measurement data collected during our vicarious field campaign in Lake Titicaca. On clear-sky days, lake surface kinetic temperatures are measured with well-calibrated TIR radiometers at multiple locations and the measurements include the times of the overpasses of Terra MODIS. Radiosonde balloons are launched on the lake shore before the MODIS overpasses to measure the atmospheric temperature and water vapor profiles. Wind speeds and surface air temperatures are also measured on the lake and at the balloon launching site. Based on the measured lake surface kinetic temperature, the water surface spectral reflectance/emissivity at MODIS viewing angle  $\theta_v$ , calculated from the refractive index of water, the measured atmospheric temperature and water vapor profiles, and the spectral radiance

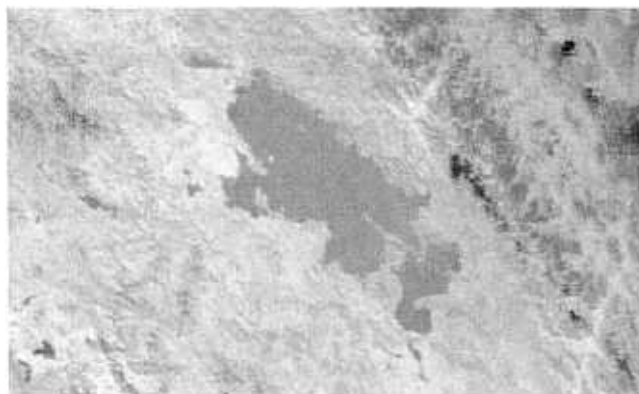


Fig. 2. MODIS color composite image covering the area of Lake Titicaca, Bolivia and Peru, on June 15, 2000, with brightness temperatures in bands 20, 29, and 31 as RGB.

at the TOA at the MODIS viewing angle  $L_\lambda(\theta_v)$  can be calculated with the state-of-art atmospheric radiative transfer model (RTM) MODTRAN4.0 (Berk et al., 1999). The band averaged radiance  $L_b(\theta_v)$  can be calculated as (Eq. (1))

$$L_b(\theta_v) = \frac{\int_{\lambda_1}^{\lambda_2} \Psi(\lambda)L_\lambda(\theta_v)d\lambda}{\int_{\lambda_1}^{\lambda_2} \Psi(\lambda)d\lambda} \quad (1)$$

where  $\psi(\lambda)$  is the spectral response function and  $\lambda_1$  and  $\lambda_2$  are lower and upper boundaries of band  $b$ , respectively. The comparison between  $L_b(\theta_v)$  and the MODIS data will give the absolute radiometric accuracy of the MODIS data in the limitations associated with the noise in the MODIS data (Wan, in press) and the uncertainty in the calculated value of  $L_b(\theta_v)$ . These limitations will be estimated by sensitivity study and error analysis.

In general, the spectral radiance coming from a non-BB surface is the combination of the surface emittance and the background radiation reflected by the surface.

$$L_\lambda(\mu) = \epsilon_\lambda(\mu)B_\lambda(T_s) + \int_0^{2\pi} \int_0^1 \mu' f_r(\mu; \mu', \phi') L_\lambda(-\mu', \phi') d\mu' d\phi' \quad (2)$$

where  $\mu = \cos \theta$ ,  $B_\lambda(T_s)$  is the Planck function at surface temperature  $T_s$ ,  $L_\lambda(-\mu', \phi')$  is the background radiance going to the surface in direction  $-\mu'$  and azimuth plane  $\phi'$ . The directional emissivity  $\epsilon_\lambda(\mu)$  and surface bidirectional reflectance distribution function (BRDF)  $f_r$  are coupled by Kirchhoff's law (Eq. (3))

$$\epsilon_\lambda(\mu) = 1 - \int_0^{2\pi} \int_0^1 \mu' f_r(\mu; \mu', \phi') d\mu' d\phi'. \quad (3)$$

In the MODTRAN4.0 code, the surface is treated as Lambertian for downward solar and atmospheric radiation when user-defined spectral reflectance values are input in a file for the surface, reflecting the downward atmospheric



Fig. 3. A photo of the floating system for a TIR radiometer used in the lake surface temperature measurements on June 15, 2000.

and solar radiations incident at any angle into all directions equally. Kirchhoff’s law then becomes (Eq. (4))

$$\epsilon_{\lambda}(\mu) = 1 - \rho_{\lambda}(\mu) \tag{4}$$

where  $\epsilon_{\lambda}$  is the spectral emissivity and  $\rho_{\lambda}$  is the spectral reflectance, which equals  $\pi f_r$  under the Lambertian assumption. Then, the integral without a constant  $f_r$  in Eq. (2) becomes the total irradiance  $E(\lambda)$ , which is the sum of the atmospheric thermal irradiance  $E_a(\lambda)$  and the total solar irradiance  $E_s(\lambda)$ . Eq. (2) becomes Eq. (5)

$$L_{\lambda}(\mu) = \epsilon_{\lambda}(\mu)B_{\lambda}(T_s) + \frac{[1 - \epsilon_{\lambda}(\mu)]}{\pi} [E_a(\lambda) + E_s(\lambda)] \tag{5}$$

In order to make an appropriate simulation of the specular reflectance for a flat lake surface under calm condition or low wind speeds, minor modifications have been made in the MODTRAN4.0 code to add an option for a specular surface with user-defined spectral reflectance values so that

$$L_{\lambda}(\mu) = \epsilon_{\lambda}(\mu)B_{\lambda}(T_s) + [1 - \epsilon_{\lambda}(\mu)]L_{\lambda}(-\mu, \pi) \tag{6}$$

as long as the viewing angle is far away from the specular reflecting angle of the incident solar beam (Eq. (6)).

We use IR radiation pyrometers (model KT15) manufactured by Heitronics and purchased through Wintronics as IR radiometers for the lake surface temperature measurements. The temperature measurement accuracy is specified as 0.5 °C plus 0.7% of the temperature difference between ambient and target in a wide temperature range from – 50 to 150 °C. The excellent performance of this instrument is due to Heitronics’ unique and patented “chopped radiation method,” which eliminates thermal drift, combined with sophisticated noise reduction signal processing circuits (refer to <http://wintron.com/Infrared/choprad.htm>). An optical chopper is used to periodically intercept the incident radiation from the measured target to the detector. During each interruption, the detector is exposed to a reference radiation from an internal BB, which temperature is measured by a high-precision thermistor. The detector response time is 1 s. The IR radiometer is powered by a 24-V battery. We store its measurement data with a stand-alone, voltage data logger from Onset Computer. The recorded voltage values are converted to temperature values in steps of 0.2 K, giving a quantitation error of 0.1 K. Routine calibrations with a liquid-bathed BB at temperatures from 0 to 50 °C indicate that the accuracy of the IR radiometer is better than 0.2 K. The liquid-bathed BB is calibrated in the laboratory by a FT-spectroradiometer MR100, a new generation of the AERI (Revercomb et al., 1993) manufactured by Bomem. The AERI is equipped with two NIST-traceable BBs at an accuracy better than 0.05 K. Because we are satisfied with the 0.2-K accuracy of the IR radiometer and it has a long-term stability of 0.01%, the measuring temperature in K/month, we do not make on-site calibrations with an external BB when field campaigns are conducted in remote areas. The IR radiometer is wrapped with aluminum sheet to prevent the instrument body from heating in the sunshine. During the deployment for lake

surface temperature measurements, each IR radiometer is supported by a floating system as shown in Fig. 3. The floating system is built with plastic tubes (1-in. diameter and 60-in. long each) and basketballs. Four plastic tubes form a rectangular. Two semicircles of plastic tubes joined together are connected to the diagonal corners. Four basketballs are connected to the corners to provide the floatation for the system. The IR radiometer mounted on the floating system looks down at a height of 75 cm above the water surface with an instant field of view (IFOV) of 32 cm in diameter. The advantages of this floating system include its light weight for easy transportation by a small boat, small cross-sections in the water so that its disturbance on the water surface is minimal, and small cross-sections in the air so that its effect on the radiometric measurement is negligible.

The calculated spectral emissivity of a flat water at view angle 8.1°, the averaged viewing angle within the radiometer’s IFOV, is shown in Fig. 4. Note that in the whole viewing angle range (0–12°) within the IFOV, the water surface emissivity almost does not change with wind speed (Masuda, Takashima, & Yakayma, 1988). The RSR of the IR radiometer using a 10–13- $\mu$ m filter and lake surface emissivities at three viewing angles by the MODIS are also shown in Fig. 4.

In the calibration of the IR radiometer with a BB at temperature  $T_{bb}$ , the temperature measured by the IR radiometer is related to the BB radiance by (Eq. (7))

$$L_H(T_{bb}) = \frac{\int_{\lambda_1}^{\lambda_2} \Psi_H(\lambda)B_{\lambda}(T_{bb})d\lambda}{\int_{\lambda_1}^{\lambda_2} \Psi_H(\lambda)d\lambda} \tag{7}$$

where  $\Psi_H(\lambda)$  is the spectral response function of the Heitronics radiometer and  $\lambda_1$  and  $\lambda_2$  are lower and upper boundaries of the response function.

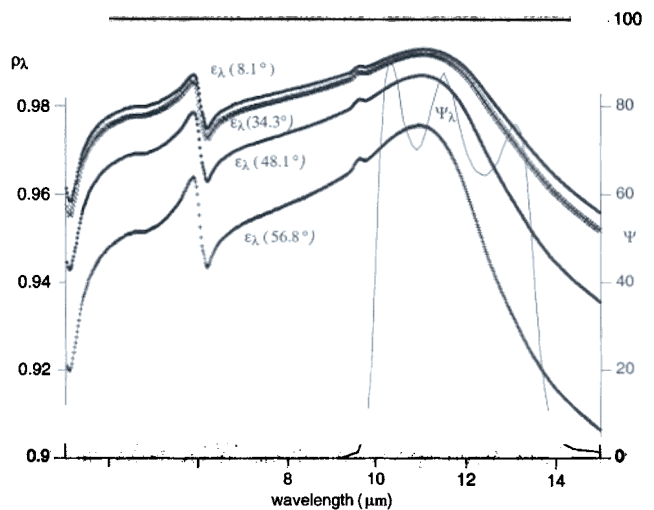


Fig. 4. The spectral emissivity of a flat water surface at four angles (8.1°, 34.3°, 48.1°, and 56.8°) and the RSR function of the Heitronics IR Radiometer using a 10–13- $\mu$ m filter.

In the lake surface temperature measurements, the radiance that the IR radiometer receives at 75 cm above a flat lake surface  $L_H(\theta_H)$  can be calculated as (Eq. (8))

$$L_H(\theta_H) = \frac{\int_{\lambda_1}^{\lambda_2} \Psi_H(\lambda) L_\lambda(\theta_H) d\lambda}{\int_{\lambda_1}^{\lambda_2} \Psi_H(\lambda) d\lambda} \quad (8)$$

where  $L_\lambda(\theta_H)$  is the radiance at the level of the IR radiometer calculated by the modified MODTRAN4.0 code for lake surface kinetic temperature  $T_s$  and a typical atmospheric temperature and water vapor profiles measured during the field campaign at Lake Titicaca.  $L_\lambda(\theta_H)$  is very close to  $\epsilon_\lambda(8.1^\circ) B_\lambda(T_s)$  because both the absorption in the 75-cm long atmospheric path and the downward atmospheric radiance at  $8.1^\circ$  from nadir in the spectral range 10–13  $\mu\text{m}$  are small and the effects of variations in the atmospheric conditions are negligible in dry atmospheric conditions. The value of  $L_H(\theta_H)$  is related to temperature  $T_H$ , and the difference between  $T_s$  and  $T_H$  is 0.7 K. This is the effect of water emissivity on measurements with the IR radiometer. Based on the conditions at the test site, this value (0.7 K) was used to get the true lake surface kinetic temperature values from the IR radiometer data during the entire field campaign. Note that the term “lake surface temperature” means “lake surface kinetic temperature” in this paper.

A radiosonde system (that consists of receiver/processor PP15, antenna RM20, and radiosonde sensor RS80) manufactured by Vaisala is used to measure the atmospheric temperature and water vapor profiles. The technical specifications of the radiosonde system are summarized as follows: pressure measurement resolution 0.1 hPa and precision 0.5 hPa in the range of 3–1060 hPa, temperature measurement resolution 0.1  $^\circ\text{C}$ , and precision 0.2  $^\circ\text{C}$  in the range from  $-90$  to  $60$   $^\circ\text{C}$ , relative humidity (RH) measurement resolution 1% RH and precision 3% RH in the range of 0–100% RH. A temperature-dependent correction was made to the radiosonde RH measurements from Vaisala RS80-A thin-film capacitive sensors due to the problems at cold temperature (Miloshevich, Vömel, Pauknen, Heymsfield, & Oltmans, 2001).

For the purpose of vicarious calibration of satellite TIR data, we need to avoid cirrus because we cannot accurately measure the cirrus optical depth and ice particle size distribution. We only used the in situ measurement data in days without cirrus clouds to estimate the calibration accuracy of MODIS TIR bands.

We conducted lake surface temperature measurements only in low wind speed conditions in clear-sky days for safety reasons. As shown in Fig. 3, the lake surface was basically flat in a low wind speed condition (0.2–0.5 m/s) on June 15 and the blue sky indicates it was a clear-sky day. For a flat lake surface, we can use the specular reflectance option in the modified MODTRAN4.0 code

to calculate the TOA radiances from measured surface and atmospheric conditions.

The scan mirror and fixed optics (including dichroic beamsplitters and filters) in the MODIS instrument are polarized. The IR radiance from water surface becomes partially polarized at oblique viewing angles through both emission and reflection (Shaw, 1999). The calibration of MODIS TIR bands is based on unpolarized sources of onboard BB and space scene, and only the total scene radiance is considered in the generation of the MODIS L1B product, ignoring the scene polarization. For consistency, we used the unpolarized water emissivity, which is the average of polarization emissivities, in the calculation of the total TIR radiance from lake surface and did not consider polarization in the atmospheric radiative transfer simulations. If we conducted in situ measurements in clear-sky lake areas simultaneously observed by the MODIS at or near nadir viewing angles, the TIR radiance from lake surface is unpolarized, satisfying the unpolarized scene assumption used in the MODIS L1B processing. However, we often had clear-sky lake scenes only at large viewing angles for the MODIS observations. In such cases, an error may be introduced in the calibration of MODIS TIR data by the unpolarized scene assumption. We should be able to evaluate the magnitude of this error when we have enough in situ measurement data in clear-sky scenes to check the calibration accuracies at nadir and large viewing angles.

#### 4. Results

We conducted a field campaign in Bolivia from May 26 to June 17, 2000. Lake surface temperature measurements were made over a wide open water area of the small portion of Lake Titicaca by the Village of Huatajata, La Paz, Bolivia in clear-sky days. The dimension of the open water area is 35 km in the E–W direction and 15 km in the S–N direction.

The weather conditions in the area of Lake Titicaca, Bolivia during the field campaign are summarized in Table 2. We made more than eight sets of in situ measurements covering the daytime or nighttime Terra overpasses under clear-sky conditions. These include May 29 day and night, June 3 day, June 4 day and night, June 13 day, June 14 night, and June 15 day in local time. Table 2 also lists the overpass time, granule ID, and sensor and solar zenith and azimuth angles of the available MODIS data over Lake Titicaca in columns 7–12. Note that all MODIS calibrated radiance data used in this study are produced by Level-1B code, version 2.5.4. Because the sky was filled with scattered clouds June 15 night and there were more clouds on June 16 and 17, we did not extend our field campaign. According to MODIS data, June 23 was the first clear-sky day in the lake area after this field campaign.

Before June 6, 2000, the radiosonde system was deployed in our LST validation field campaign in Uyuni

Table 2  
Summary of weather conditions and MODIS data over Lake Titicaca, Bolivia during the May 29–June 15, 2000 field campaign

Date (mm/dd)	Cloud by		Wind speed (m/s)	Rain	Radiosonde data	MODIS				Solar zenith (°)	Solar azimuth (°)
	visual observation	Condition in MODIS data				overpass (UTC)	MODIS granule ID	Sensor zenith (°)	Sensor azimuth (°)		
05/29	in SW				No	14:43	150.1440	49.8	99.9	46.2	35.9
05/30	clear		2		No	02:56	151.0255	56.9	83.9		
05/31	partly				No						
06/01	cloudy		7	rain							
06/02	cloudy		11		No						
06/03	clear		4–6		No	15:02	155.1500	19.6	98.5	44.6	30.7
06/04	clear		1–3		No	15:45	156.1540	57.8	–83.5	40.5	17.4
06/05	clear		2–3		No	03:57	157.0355	51.3	–100.2		
06/06	cloudy				No						
06/07	cloudy				No						
06/08	cloudy			rain							
06/09	cloudy			rain							
06/10	cloudy			rain							
06/11	cloudy				No						
06/12	cloudy				Yes						
06/13	in NW		0.3		Yes	15:39	165.1535	51.6	–83.0	41.8	19.6
06/14	partly				No						
06/15	in NE		2–4		Yes	02:56	167.0255	56.8	83.2		
06/15	clear		0.5		Yes	15:26	167.1525	34.3	–82.7		23.6

Salt Flats, Bolivia. We deployed the radiosonde system and launched radiosonde balloons on the shore of Lake Titicaca at the Village of Huatajata, La Paz, Bolivia to measure the atmospheric temperature and water vapor profiles after June 6, 2000. Two balloons were launched each day on June 12, 13, and 15, 2000. June 12 was a cloudy day and we launched two balloons to test the radiosonde system. On June 13, the first balloon launched at 14:22 UTC was unsuccessful. The second was launched at 16:57 UTC after the MODIS overpass time and reached 13.7 km above sea level after 1 h. The surface wind speed was around 0.3 m/s. The column water vapor integrated from the water vapor profile (without the temperature-dependent correction) is 0.448 cm. On June 15, the first balloon was launched at 02:16 UTC (local time 22:16 h, June 14) 39 min before the MODIS overpass time and the second at 15:00 UTC (local time 11:00 h, 15 June) 26 min before the MODIS overpass. The first radiosonde balloon reached 16 km above sea level and the surface wind speed was 2–4 m/s. The second radiosonde balloon reached 22 km above sea level under weak surface wind condition of 0.2–0.5 m/s. It gave us a chance to measure the atmospheric temperature and water vapor profiles up to the middle stratosphere. As shown in Fig. 5(a), the three measured atmospheric temperature profiles are very close to the averaged tropical atmospheric profile. There are only small differences at elevation levels from 15 to 22 km. Therefore, it is reasonable to use the averaged tropical atmospheric profile (provided in the MODTRAN code) at levels above 22 km. After making the temperature-dependent correction to the RH readings from the Vaisala RS80-A thin-film capacitive sensors (Miloshevich et al., 2001), the measured three water vapor profiles shown in Fig. 5(b) give column water vapor values

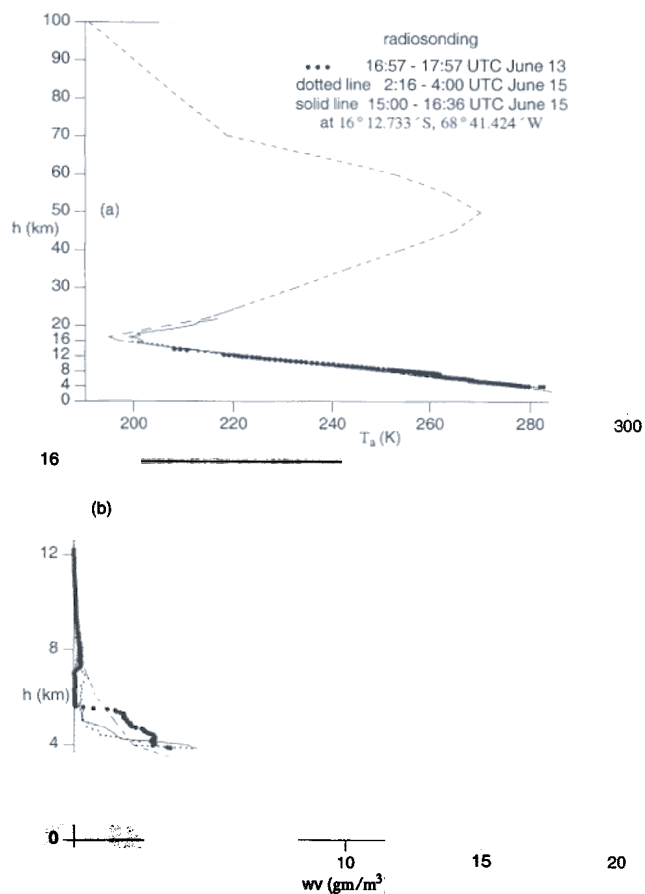


Fig. 5. Atmospheric temperature (a) and water vapor (b) profiles measured at Lake Titicaca, Bolivia on June 13 and 15, 2000 and the average tropical atmospheric profiles (dashed lines).

of 0.458, 0.242, and 0.289 cm, indicating very dry atmospheric conditions for the nighttime and daytime MODIS overpasses in these 2 days.

It is interesting to point out that the radiosonde balloon launched at 02:16 UTC, June 15 (before the nighttime MODIS overpass, at local time June 14 night), experienced a tough time before it burst at 16 km above sea level. Fig. 6 shows the balloon speed at the altitude it reached and the measured atmospheric temperature profiles for the nighttime and daytime radiosondes launched on June 15. The balloon launched at 15:00 UTC was bounced up and down a few times at 8 km altitude and then it moved up smoothly at a speed of 3–4 m/s until it burst at 22 km. The balloon launched at 02:16 UTC moved normally at a speed around 2 m/s up to 10 km altitude, then the speed was doubled at about 11 km. At altitude above 11 km, the balloon was bounced up and down many times until it burst at 16 km. Its maximum upward speed was 18 m/s and downward speed was about  $-28$  m/s, indicating a large-scale air mass rising motion at the high altitude. Fig. 6(b) shows that in the early

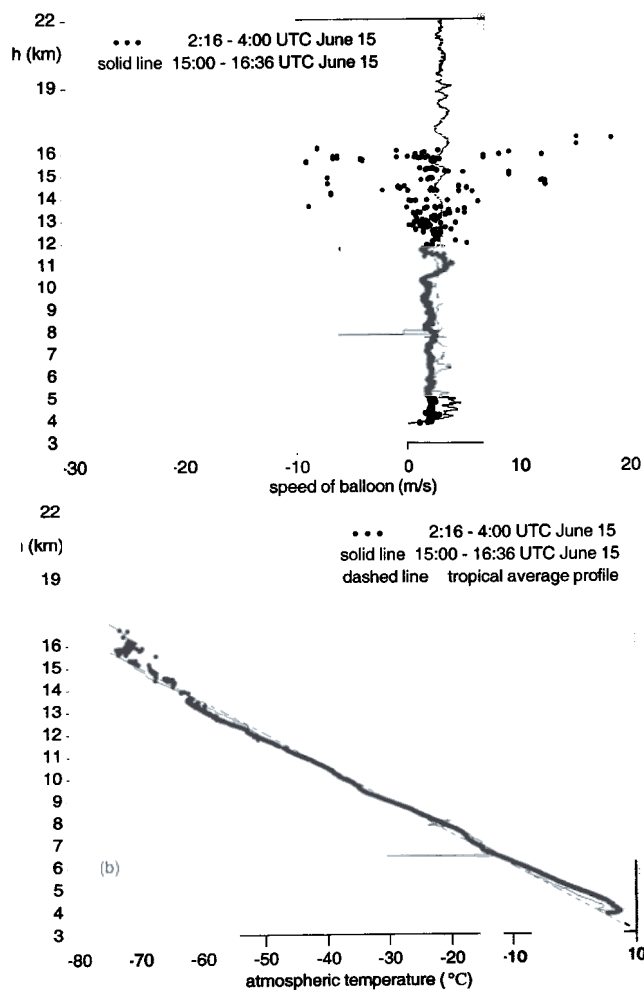


Fig. 6. The radiosonde balloon speed (a) and the measured atmospheric temperature profiles (b) in nighttime and daytime launches on June 15, 2000.

morning around 02:16 UTC, there was a thin inversion layer in the atmospheric temperature just above the surface and the air temperature was slightly warmer than that in the daytime (around 16:00 UTC) by a few degree Kelvin at levels between 4 and 6 km. However, the temperature was a few degree cooler at the altitude between 11 and 13 km and 2–4 K warmer at the altitude between 14 and 16 km, indicating the strong warm and cold temperature perturbations in the early morning.

In situ measurements (McFarquhar, Heymsfield, Spenshirne, & Hart, 2000) and radiosonde observations (Boehm & Verlinde, 2000) revealed the high occurrence of thin and subvisual tropopause tropical cirrus and the evidence that tropical waves play a role in the life cycle of tropical cirrus by providing a source of rising motion and cooling. Numerical experiments (Starr & Cox, 1985) show that there are significant differences in maintained ice water content and cloud structure between simulated cirrus under midday and nighttime conditions with the cloud appearing more cellular but less dense overall in midday conditions.

Because the radiosonde data showed the evidence of air rising motion, and the warm and cold temperature perturbations for the nighttime MODIS overpass on June 15, we expect to see the effect of subvisual thin cirrus in the MODIS TIR data.

We deployed eight temporary buoys (each made of a basketball, rope, and rocks) during the field campaign (see Fig. 3). One thermistor-datalogger system was connected to each buoy and the thermistor was placed about 1 cm beneath the water surface. Five IR radiometers were connected to the buoys in the middle. They were all far away from the lake shore at a distance larger than 3 km. Four IR radiometers were connected to the buoys at the corners of a parallelogram, about 1 km long in the N–S side and 1.5 km long in the E–W side. Another one was connected to the middle buoy. As shown in Fig. 7, the orientation of the parallelogram was almost parallel to the daytime Terra orbit, with buoy locations marked in small circles. The latitude and longitude values of buoy locations for the radiometers are also given in Fig. 8.

After comparing all the cases, we found that the June 15 daytime data set provides the best data set for the evaluation of MODIS TIR calibration because of the following reasons: clear atmosphere all over the sky, wind speed of 0.2–0.5 m/s before, during, and after the Terra overpass, successful in situ measurements of the lake surface temperature and balloon release, and the MODIS viewing angle  $34.3^\circ$ . Besides the continuous measurements of the lake surface temperatures by five IR radiometers at the buoy positions, the spatial distribution of lake surface temperature was also measured on June 15 by an IR radiometer, which was placed in the front of a moving boat. The radiometer was about 2 m away from the boat edge so that it can measure the lake surface temperature before the surface was disturbed by the waves caused by boat's movement. As shown in Fig. 8(a), this IR radiometer gave the lake surface temperature on the

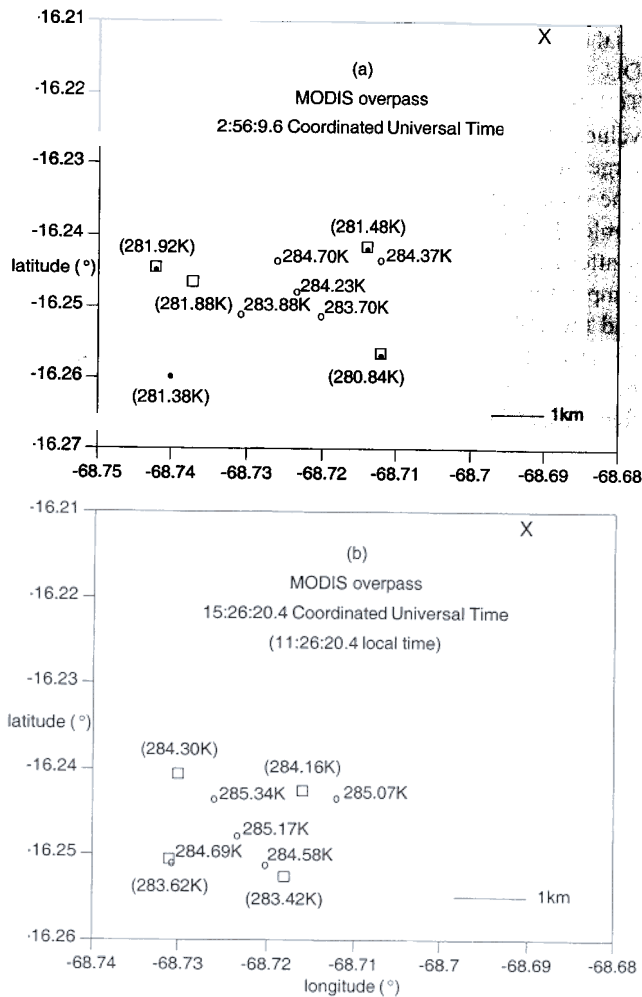


Fig. 7. The geolocations of IR radiometers (circle) and MODIS pixel centers (square and bullet) over Lake Titicaca and the site for launching radiosonde balloons (cross) on June 15, 2000.

way from our base on the lake shore in Huatajata to the buoy positions listed in Fig. 8(b–f). The last radiometer was deployed around 09:42 h local time. Then, the boat moved away to the west by 1.5 km so that the area covered by buoys would not be disturbed by boating during the Terra overpass. Note that the thermistor at the buoy position in Fig. 8(b) was lost and that the difference between the lake surface kinetic temperatures measured by the IR radiometers after the emissivity correction and bulk temperatures measured by thermistors about 1 cm beneath the water surface is slightly larger than 1 K. Therefore, it is not appropriate to convert the bulk temperatures to the TOA radiance through atmospheric radiative transfer calculations without measuring the temperature gradient at the lake surface. This large difference between surface kinetic temperature and bulk temperature is due to the low wind speed. The temperature difference reduced to 0.8 K in the daytime case on June 3 when the wind speed was 4–6 m/s.

For the pixels around our buoy positions at Lake Titicaca on June 15, 2000, the nighttime MODIS Geolocation file

MOD03.A2000167.0255.002.2000171040355.hdf gives viewing zenith angle  $56.8^\circ$  from the east for the Earth view time 02:56 UTC. The daytime MODIS Geolocation file MOD03.A2000167.1525.002.2000183215414.hdf gives viewing zenith angle  $34.3^\circ$  from the west (azimuth angle  $-82.7^\circ$ ), solar zenith angle  $43.0^\circ$ , and azimuth angle  $23.6^\circ$  for the Earth view time 15:26:20 UTC.

As shown in Fig. 8, there are fluctuations in the lake surface temperatures measured by the IR radiometers. The data recording rate of the IR radiometers is one sample every 2 s. We believe that these high-frequency fluctuations in the lake surface temperatures are the effects of wind, waves, and currents at the scales around 75 cm (the size of IFOV of the radiometer). Because we are interested in the lake surface temperature at larger scales from 100 m to 1 km, the size of a MODIS pixel, the lake surface temperatures averaged in a time interval of the MODIS overpass  $\pm 1$ –5 min will represent the lake surface temperature in a small area surrounding the positions of the IR radiometers. These averaged lake surface temperatures are given near the positions (represented by symbol circle) of the five IR radiometers in Fig. 7. The numbers in parentheses above

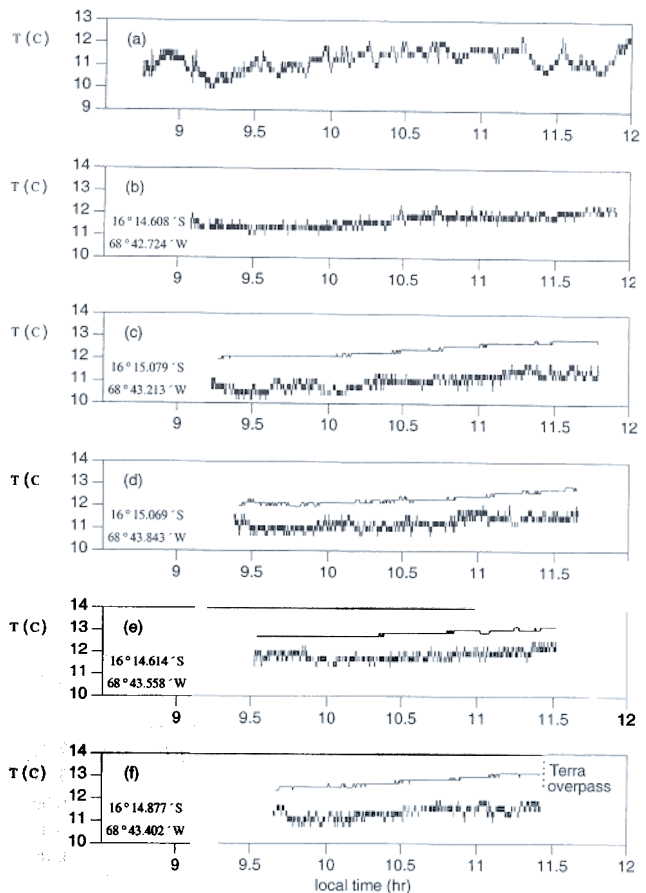


Fig. 8. Lake surface temperatures measured with an IR radiometer carried by boat (a) and IR radiometers (heavy lines) and thermistors (thin lines) by floating systems (b–f) at buoy positions on June 15, 2000. Note that the thermistor at the position in (b) was lost.

or below the square symbols are the brightness temperatures in band 31 from the MODIS L1B data. In Fig. 7(a) for the nighttime overpass, the four bullet symbols represent the centers of pixels in scan lines 490 and 491, while the square symbols represent the centers of pixels in scan lines 491, 490, and 487 that are closest to the averaged buoy position because of the bowtie effect by the end of swath (sensor zenith angle at 56.8°). In Fig. 7(b) for the daytime overpass, the two square symbols in the upper positions are the centers of pixels in scan line 523 (viewed by the fourth channel or detector element in each band) and the square symbols in the lower positions represent the centers of pixels viewed by the fifth detector in each band.

Before making detailed comparisons, we need to make a sensitivity study for the following reasons. As shown in Table 2, we only have three sets of radiosonde data in clear-sky conditions (possibly with thin cirrus for the nighttime data set). We want to know what is the effect of the problem with RH measurements of the radiosonde at cold temperatures and for which TIR bands it is appropriate to apply the measured atmospheric temperature and water vapor profiles to the MODIS data in the large portion of Lake Titicaca on the same days and to the in situ lake surface temperature data on other days. The daytime atmospheric temperature and water vapor profile measured on June 15 up to 22 km altitude combined with the averaged tropical atmospheric profile above 22 km was used as the base profile in the sensitivity study with the MODTRAN4.0 code. The mean tropical profiles of atmospheric compositions including ozone, carbon dioxide, methane, nitrous oxide, nitric acid, and other trace gasses were also used in the radiative transfer simulations. The column ozone integrated from the averaged tropical atmospheric ozone profile is 0.266 ATM CM (equivalent to 266 Dobson units). The EP/TOMS

total ozone map on June 15, 2000 gives a range of 250–275 DU for the Lake Titicaca region (thanks to the NASA TOMS webpage <http://toms.gsfc.nasa.gov>). The error in values of the TOMS total ozone map may be significantly larger than a few percent (Chesters & Neuendorffer, 1991). The simulation results for the sensitivity study are shown in Table 3. The effect of standard cirrus (absorption and scattering) with optical depth 0.007 on the brightness temperature in MODIS TIR bands is shown in column 2, and the effect of thin subvisual cirrus in the same optical depth is shown in column 3. Note that there is a forward peak in the scattering of cirrus and the absorption effect of thin cirrus is much stronger in long wavelengths. The values in columns 4–8 are the effects of variations in atmospheric conditions: temperature variation  $\delta T_a$  of 0.5 K, water vapor variation  $\delta wv$  of 10%, set RH to 30% at levels between 9 and 12 km altitude (column 6), CO<sub>2</sub> variation by 10 ppm, and O<sub>3</sub> variation by –6%, respectively. The viewing zenith angle is 56.9° for the case in column 8 and 34.3° for all other cases. The effects of variations in water vapor in columns 5 and 6 indicate that the calibration of MODIS water vapor bands 27 and 28 cannot be validated with the water vapor profile measured by Vaisala RS80-A radiosondes because of its problem at cold temperatures (Miloshevich et al., 2001). The effects of increasing lake surface kinetic temperature by 0.25 K are shown in column 9, and effects of changing lake surface from a flat mirror surface (for specular reflectance) to a completely rough surface with random slopes and aspects (for Lambertian reflectance) are shown in columns 10 and 11 in night and day cases, respectively. The  $\delta T_b$  value required to meet the specified radiometer accuracy in MODIS TIR bands is also given in column 12. From this sensitivity study, we can get the following insights into the requirements for field campaigns

Table 3

Sensitivities of the calculated MODIS TIR band brightness temperatures on the variations in the surface and the atmospheric conditions and the  $\delta T_b$  (K) values required for the specified radiometric accuracies

Band no.	Visible cirrus 64- $\mu$ m mode	Subvisual cirrus 4- $\mu$ m mode	$\delta T_a$ 0.5 (K)	$\delta wv$ 10%	Set RH 30% (9–12 km)	$\delta CO_2$ 10 ppm	$\delta O_3$ –6% ( $\theta_v$ 56.9°)	$\delta T_s$ 0.25 (K)	Surface S → L night ( $\theta_v$ 34.3°)	Surface S → L day ( $\theta_s$ 43°)	$\delta T_b$ (K) for specified radiometric accuracy (%)
20	–0.15	–0.18	0.02	–0.02	0.02				0.01	4.80	0.16 (0.75)
21	–0.16	–0.20	0.02						0.01	2.55	2.23 (10)
22	–0.16	–0.19	0.02						0.02	2.71	0.22 (1)
23	–0.16	–0.20	0.04			–0.01			0.02	1.99	0.22 (1)
24	–0.18	–0.23	0.26			–0.10			0.02	0.13	0.20 (1)
25	–0.18	–0.24	0.16	–0.01		–0.01	0.01		0.04	0.27	0.22 (1)
27	–0.27	–0.34	0.48	–0.69	–4.29						0.30 (1)
28	–0.30	–0.36	0.37	–0.47	–1.41			0.04	0.03	0.02	0.36 (1)
29	–0.25	–0.36	0.04	–0.05	–0.05		0.01	0.23	0.04	0.03	0.47 (1)
30	–0.40	–0.28	0.18	–0.01	–0.01		0.55	0.16	0.04	0.03	0.47 (1)
31	–0.44	–0.30	0.02	–0.03	–0.01			0.24	0.02	0.01	0.31 (0.5)
32	–0.49	–0.46	0.02	–0.04	–0.02			0.24	0.05	0.04	0.33 (0.5)
33	–0.54	–0.60	0.17	–0.04	–0.09	–0.19	0.04	0.15	0.21	0.12	0.65 (1)
34	–0.56	–0.62	0.27	–0.02	–0.04	–0.28	0.03	0.07	0.13	0.09	0.61 (1)
35	–0.56	–0.64	0.33	–0.01	–0.01	–0.26	0.04	0.04	0.07	0.05	0.58 (1)
36	–0.68	–0.66	0.40	–0.01	–0.04	–0.27		0.01			0.53 (1)

to validate the calibration accuracies of MODIS TIR bands. Firstly, for the bands in atmospheric windows (i.e., bands 20–23, 29, and 31–32), the effects due to uncertainties in atmospheric temperature and water vapor profiles are equal or smaller than instrument's NEDT in the high altitude site in dry seasons. The accuracy in measured lake surface kinetic temperatures is the limiting factor. The effect of lake surface roughness related to surface wind speed is very small at night. The water bulk temperature in the surface layer of about 1 cm thick measured by thermistors will be close to the surface kinetic temperature in high wind speed conditions. However, it is not safe to deploy radiometers in the lake under high wind speed conditions, especially at night. Low wind speed conditions are required in daytime cases in order to avoid the difficulty to deal with the reflected solar radiation in bands 20–23. The effects of these uncertainties are larger in band 33 but are still significantly smaller than 1%, the specified calibration accuracy for TIR bands. Secondly, for these atmospheric window bands, it may be possible to apply the measured atmospheric temperature and water vapor profiles to other sites about 60 km away from the radiosonde launch site or to other days in a period of a few weeks as long as the sky is clear in all directions and there is no significant changes in the surface atmospheric conditions (air temperature, RH, and wind speed). However, an overall consistency check and error analysis must be made for all possible effects of the variations and uncertainties in atmospheric conditions. Thirdly, for the atmospheric temperature sounding bands (i.e., bands 24–25 and 34–36), real-time in situ measurements of atmospheric temperature and water vapor profiles are required. The effects of temporal and spatial variations in the measured atmospheric temperature and water vapor profiles may be too large to validate the calibration accuracy at the 1% level. Lastly, it is difficult to validate band 30 (the ozone band) without in situ measurement of the ozone profile.

According to the above insights and the weather conditions listed in Table 2, we decided that (1) the estimate of

calibration accuracy will be made only for eight MODIS bands, i.e., bands 20–23, 29, and 31–33; (2) the three MODIS overpass cases on June 13 and 15 will be our primary cases; (3) the daytime atmospheric temperature and water vapor profile measured on June 15 will be used for the May 29 case. However, the June 3 daytime case will not be used because of the relatively high wind speed. The June 4 daytime case will also not be used because the measured air surface temperature was about 3 K warmer. (4) The nighttime atmospheric temperature and water vapor profile measured on June 15 will be used for cases of May 30 and June 5. Lastly, (5) the daytime and nighttime atmospheric temperature and water vapor profiles measured on June 15 will be used for sites in the large portion of Lake Titicaca, where brightness temperatures in band 31 are highly uniformed so that we can check the effects of the instrument noise and the spatial variation in MODIS TIR data on the comparison between MODIS TIR data and the calculated TOA radiances based on the measured lake surface kinetic temperatures and atmospheric profiles. We decided to make comparisons in more cases because we have to consider many factors related to the estimate of calibration accuracy, including sensor NEDT and spatial variations in MODIS data, sensor response across scan, viewing angle-dependent scene polarization, and possible thin subvisual cirrus.

We first compare the June 15 daytime data set. The averaged latitude and longitude of the five IR radiometers is 16.247°S and 68.723°W. The averaged lake surface kinetic temperature measured by five IR radiometers after the correction for the emissivity effect is 11.82 °C (284.97 K) at the MODIS observation time. Combined with the measured atmospheric temperature and water vapor profiles, we can calculate the TOA spectral radiance at the MODIS viewing angle. Because of the low surface wind speed (less than 0.5 m/s), there were only small ripples over the lake surface so that the lake is basically flat. Therefore, we used the option for a specular surface in the modified MODTRAN4.0 code with the water reflectance at view angle

Table 4

Comparisons between MODIS TIR band brightness temperatures ( $T_b$ ) and the calculated TOA  $T_b$  values (K) in three daytime cases over Lake Titicaca, Bolivia on May 29 and June 13 and 15, 2000

Band	June 15, 15:26 UTC, A2000167.1525, $T_s=284.97$ K (523, 1052), 16.247 °S, 68.723°W, $\theta_v=34.3^\circ$ , $\phi_v=-82.7^\circ$ , $\theta_s=43.0^\circ$ , $\phi_s=23.6^\circ$			June 13, 15:39 UTC, A2000165.1535, $T_s=284.75$ K (1458, 1229), 16.247 °S, 68.723 °W, $\theta_v=51.6^\circ$ , $\phi_v=-83.0^\circ$ , $\theta_s=41.8^\circ$ , $\phi_s=19.6^\circ$			May 29, 14:43 UTC, A2000150.1440, $T_s=285.92$ K (1440, 142), 16.246 °S, 68.720 °W, $\theta_v=49.8^\circ$ , $\phi_v=99.9^\circ$ , $\theta_s=46.2^\circ$ , $\phi_s=35.9^\circ$		
	Calculated $T_b$ (K)	MODIS $T_b$ (K)	MODIS – calculated $T_b$ (K)	Calculated $T_b$ (K)	MODIS $T_b$ (K)	MODIS – calculated $T_b$ (K)	Calculated $T_b$ (K)	MODIS $T_b$ (K)	MODIS – calculated $T_b$ (K)
283.67			+0.49	282.75		+0.76	284.12		+0.59
283.15			+0.23	282.21		+2.58	283.42		+0.89
283.19			+0.11	282.26		+0.50	283.49		+0.27
281.89			+0.01	280.59		+0.34	281.79		+0.46
282.14			+0.07	280.47		+0.24	282.08		-0.09
283.82			+0.07	282.71		+0.36	284.15		+0.18
283.50			-0.19	282.00		-0.02	283.55		-0.28
266.69			+0.51	263.41		+0.49			

Table 5  
Comparisons between MODIS TIR band brightness temperatures ( $T_b$ ) and the calculated TOA  $T_b$  values (K) in four nighttime cases over Lake Titicaca, Bolivia and Peru, on May 30 and June 5, 15, and 23, 2000

Band	June 15, 2:56 UTC, A2000167.0255, $T_s=284.18$ K (491, 1279), 16.247°S, 68.723°W, $\theta_v=56.8^\circ$ , $\phi_v=83.2^\circ$			June 5, 3:57 UTC, A2000157.0355, $T_s=284.79$ K (1023, 128), 16.251°S, 68.724°W, $\theta_v=51.3^\circ$ , $\phi_v=-100.2^\circ$			May 30, 2:56 UTC, A2000151.0255, $T_s=285.69$ K (519, 1280), 16.252°S, 68.726°W, $\theta_v=56.9^\circ$ , $\phi_v=83.9^\circ$			June 23, 3:45:21 UTC, A2000175.0345, $T_s=285.01$ K (142, 366), 15.508°S, 69.677°W, $\theta_v=28.3^\circ$ , $\phi_v=-98.6^\circ$		
	Calculated $T_b$ (K)	MODIS $T_b$ (K)	MODIS – calculated $T_b$ (K)	Calculated $T_b$ (K)	MODIS $T_b$ (K)	MODIS – calculated $T_b$ (K)	Calculated $T_b$ (K)	MODIS $T_b$ (K)	MODIS – calculated $T_b$ (K)	Calculated $T_b$ (K)	MODIS $T_b$ (K)	MODIS – calculated $T_b$ (K)
20	281.99	281.99	+0.00	282.99	282.42	-0.57	283.42	283.62	+0.20	283.81	284.31	+0.50
21	281.18	281.89	+0.71	282.29	281.93	-0.36	282.59	282.22	-0.37	283.33	283.20	-0.13
22	281.25	281.57	+0.32	282.35	281.99	-0.36	282.67	283.12	+0.45	283.36	284.00	+0.64
23	279.41	279.68	+0.27	280.70	280.41	-0.29	280.74	281.24	+0.50	282.17	282.70	+0.53
29	279.69	279.19	-0.50	281.02	280.11	-0.91	281.00	280.73	-0.27	282.41	282.31	-0.10
31	281.86	281.53	-0.33	283.05	282.13	-0.92	283.28	283.13	-0.15	284.00	284.11	+0.11
32	280.91	280.25	-0.66	282.42	281.22	-1.20	282.30	281.79	-0.51	283.73	283.52	-0.21
33	261.78	262.52	+0.74									

The nighttime atmospheric profile measured on June 15 was used in all calculations because of lack of radiosonde on other dates. Note that no value is given in band 33 for these other dates.

34.3° as the user-defined spectral reflectance to calculate the TOA radiance. Because MODIS viewing angle (zenith angle 34.3° and azimuth angle -82.7°) was far away from the specular reflecting direction of the incident solar beam at zenith angle 43.0° and azimuth angle 23.6°, the solar radiation was not included in the radiative transfer calculations. The calculated spectral atmospheric transmission at viewing angle 34.3° is greater than 0.95 for most of the 3.7–4.1- and 8.13-μm atmospheric windows.

With the MODIS RSR functions, we can calculate the band brightness temperatures ( $T_b$ ) for the MODIS TIR bands. Then, we pick up the calibrated radiance values in the eight MODIS TIR bands and convert them into band brightness temperatures for the four pixels close to the locations of the five IR radiometers from the MODIS L1B data granule MOD021KM.A2000167.1525.002.2000354204307.hdf, which is generated by v2.5.4 L1B code. With 2-D interpolations, we can get the MODIS measured  $T_b$  values at the averaged position of the five IR radiometers. As shown in Table 4, we compared the calculated  $T_b$  values (in column 2) with the MODIS measured  $T_b$  values (in column 3), giving their differences in column 4. Related information and parameters are shown on the top of this table, including date, MODIS overpass time, granule ID, measured surface temperature  $T_s$ , the line and sample numbers of the pixel closest to the averaged buoy position, latitude, and longitude of the averaged position, sensor observation zenith and azimuth angles, and solar zenith and azimuth angles. As shown in column 4, the  $T_b$  difference between calculated value and the MODIS value in band 22 is 0.11 K. There are more errors in band 22 than others in this case because pixels of the fourth detector (in scan line 523) are used in the 2-D interpolation for the MODIS  $T_b$  at the averaged buoy position. Since the fourth detector in band 22 is too noisy (Wan, in press), its radiance value is replaced with

the average value of the neighboring detectors (i.e., the third and fifth) at the same sample number.

Similarly, the comparison results are shown in columns 5–7 for the June 13 daytime case where the atmospheric profiles measured by the second radiosonde balloon launched on June 13 were used in the MODTRAN calculations. For the May 29 case, the more complete atmospheric profile measured by the daytime radiosonde balloon launched on June 15 was used in the radiative transfer simulations because there were no measurements of the atmospheric profile on this day. Comparison results are shown in columns 8–10 only for the atmospheric window TIR bands. The corresponding L1B files are MOD021-KM.A2000165.1535.002.2000354201825.hdf and MOD021KM.A2000150.1440.002.2000354204059.hdf. Note the slight differences in latitude and longitude values of the averaged buoy position because only three buoys were deployed on May 29. Comparing the three cases of May 29 and June 13 and 15, the  $T_b$  difference in band 31 ranges from 0.07 to 0.36 K. We consider these numbers quite compatible because of the error contributions from in situ lake surface temperature measurements, detector noise, incomplete knowledge of sensor response across scan, and uncertainties in the temporal and spatial variations of the atmospheric profiles. Detailed error analysis will be made in Section 5.

Comparison results for four nighttime cases are given in Table 5. The first three cases shown in columns 2–10 are for June 15 and 5 and May 30. The lake surface kinetic temperatures were measured by the IR radiometers and the atmospheric profile used in MODTRAN simulations was the one measured by the radiosonde balloon launched on June 15 because of lack of radiosonde on other days. The MODIS  $T_b$  values in band 31 are all smaller than the calculated values by different amounts. The MODIS observed the buoy location at almost the same viewing angle on May 30 and June 15.

Table 6

The differences between MODIS TIR band brightness temperatures ( $T_b$ ) and the calculated TOA  $T_b$  values (in K) in six cases over Lake Titicaca, Bolivia and Peru, in May/June 2000

	May 29, 14:43 UTC, $T_s=285.92$ K	June 13, 15:39 UTC, $T_s=284.75$ K	June 15, 15:26 UTC, $T_s=284.97$ K	May 29, 14:43 UTC $T_s=286.07$ K	June 13, 15:39 UTC, $T_s=285.66$ K	June 15, 15:26 UTC $T_s=285.65$ K
	2-D interpolation with four pixels for in situ comparison			Comparison on a subarea of 10 × 16 pixels		
	(1440, 142)	(1458, 1229)	(523, 1052)	(1403, 98)	(1424, 1187)	(470, 972)
	lat. = -16.246°, lon. = -68.720°, $\theta_v=49.8^\circ$ , $\phi_v=99.9^\circ$ , $\theta_s=46.2^\circ$ , $\phi_s=35.9^\circ$	lat. = -16.247°, lon. = -68.723°, $\theta_v=51.6^\circ$ , $\phi_v=-83.0^\circ$ , $\theta_s=41.8^\circ$ , $\phi_s=19.6^\circ$	lat. = -16.247°, lon. = -68.723°, $\theta_v=34.3^\circ$ , $\phi_v=-82.7^\circ$ , $\theta_s=43.0^\circ$ , $\phi_s=23.6^\circ$	lat. = -15.583°, lon. = -69.451°, $\theta_v=53.5^\circ$ , $\phi_v=100.2^\circ$ , $\theta_s=46.5^\circ$ , $\phi_s=36.9^\circ$	lat. = -15.911°, lon. = -69.395°, $\theta_v=48.1^\circ$ , $\phi_v=-82.6^\circ$ , $\theta_s=41.8^\circ$ , $\phi_s=20.6^\circ$	lat. = -15.697°, lon. = -69.557°, $\theta_v=27.6^\circ$ , $\phi_v=-82.1^\circ$ , $\theta_s=42.9^\circ$ , $\phi_s=24.8^\circ$
Band						
20	+0.59	+0.76	+0.49	+0.65	+0.55	+0.66
21	+0.89	+2.58	+0.23	+0.52	+0.35	+0.56
22	+0.27	+0.50	+0.11	+0.75	+0.55	+0.55
23	+0.46	+0.34	+0.01	+0.73	+0.41	+0.39
29	-0.09	+0.24	+0.07	+0.10	+0.11	-0.08
31	+0.18	+0.36	+0.07	+0.18	+0.16	+0.08
32	-0.28	-0.02	-0.19	-0.24	-0.21	-0.17
33		+0.49	+0.51		+0.60	+0.50

The daytime atmospheric profile measured on June 15 was used in calculations for the May 29 case because of lack of radiosonde data on May 29. Note that no value is given in band 33 for the May 29 case.

Possible variations in the atmospheric conditions would make some contributions to the  $T_b$  difference. By comparing the spectral features in the  $T_b$  differences, we believe that the negative values of the  $T_b$  difference are mainly due to the effect of subvisual cirrus as shown in Table 3 column 3. We expected the effect of a thin subvisual cirrus in the June 15 nighttime case because of the evidence of air mass rising motion shown in the radiosonde data (Fig. 6). Occurrences of nighttime subvisual cirrus (on all three nighttime MODIS overpasses during the field campaign) are consistent with the existing in situ measurements (McFarquhar et al., 2000),

radiosonde observations (Boehm & Verlinde, 2000), and numerical experiments (Starr & Cox, 1985). Column 10 in Table 5 shows that the effect of subvisual cirrus was quite small in the nighttime case of May 30. It is interesting to compare this nighttime case with the May 29 daytime case because the time difference between these two cases is only approximately 12 h. The  $T_b$  difference values in bands 22–23 and 29 are compatible within  $\pm 0.2$  K in these two cases (Table 4 column 10 versus Table 5 column 10), supporting our conclusion based on the specular assumption for lake surface reflectance under low wind speed conditions: the

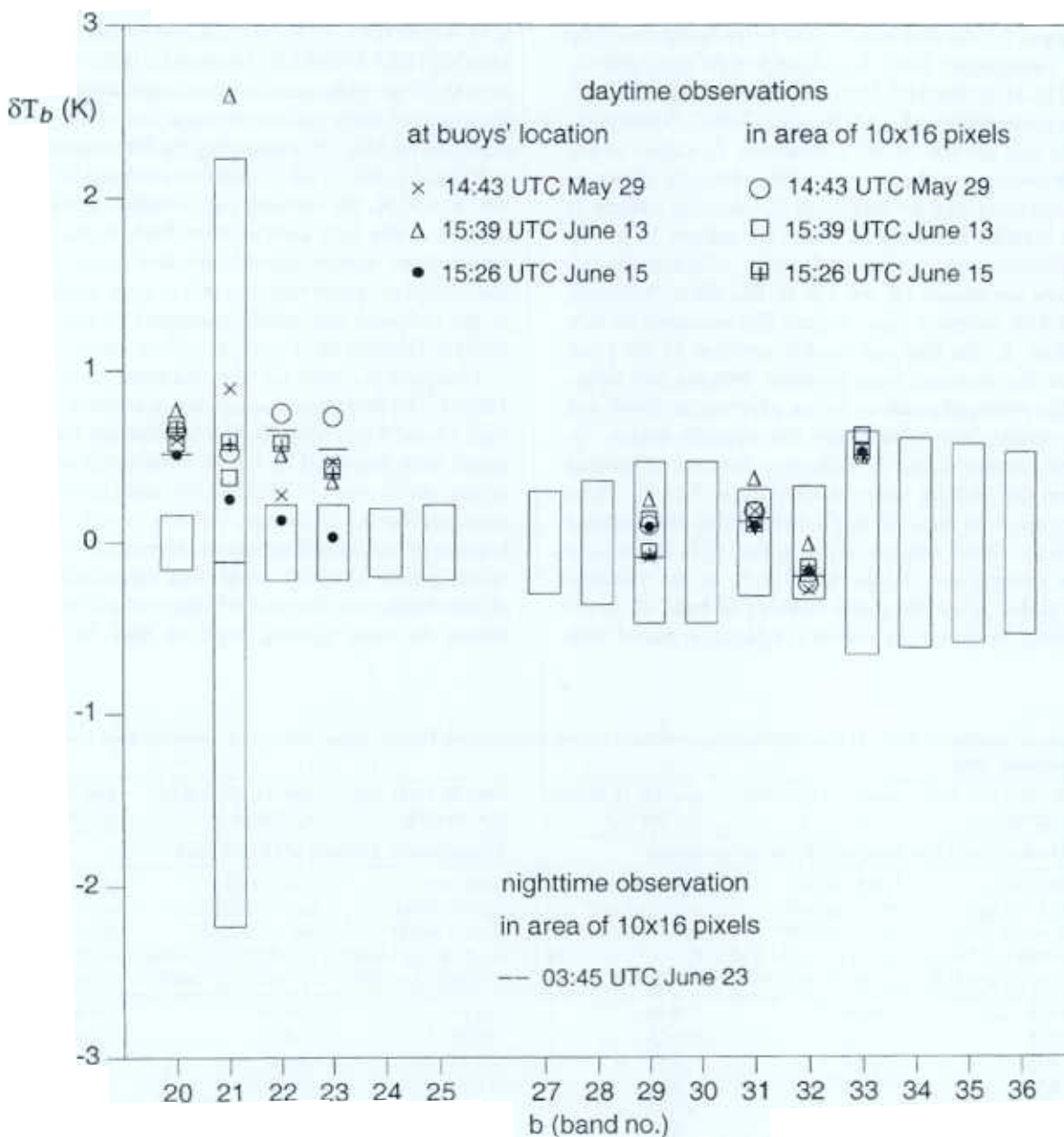


Fig. 9. The estimated calibration bias ( $\delta T_b$ ) values in MODIS TIR bands 20–23, 29, and 31–33. The estimate is not given for other bands because the RMS values of the uncertainties in the calibration accuracy estimate exceed 1%. The upper and lower boundaries of the boxes show the specified calibration accuracies.

positive values of  $T_b$  difference in bands 20–23 in daytime cases are not caused by the solar reflectance. We also compared the nighttime case of June 23 even though there is no in situ measurement for the lake surface temperature and atmospheric profile because we found a subarea of  $10 \times 16$  pixels in the large portion of Lake Titicaca where the  $T_b$  value in band 31 varies within  $\pm 0.1$  K in L1B data file MOD021-KM.A2000175.0345.002.2001004203223.hdf. We used the average  $T_b$  difference in band 31 given in Table 5 to infer the lake surface kinetic temperature of this subarea through the MODTRAN4.0 simulations based on the nighttime atmospheric profile measured 1 week earlier in our field campaign. The important point we want to make here is that the  $T_b$  difference values in this nighttime case are very compatible to the values for three daytime cases in Table 4. This will be one more reason to support our conclusion: the positive values of  $T_b$  difference in bands 20–23 are not caused by the solar reflectance. The main reason for this conclusion is that lake surface is almost flat in low wind speed conditions and the MODIS instrument observed the location of interest far from the specular reflecting direction of the sun in the three daytime cases. There is another reason to support this conclusion. If the solar reflectance made significant contributions to the positive value  $T_b$  difference in bands 20–23, the value in band 20 should be much larger than the values in bands 22 and 23 as shown in Table 3 column 11 because of stronger solar irradiance and stronger reflectance in band 20 (reflectance being 1 minus emissivity shown in Fig. 4).

As mentioned earlier, the error sources in the direct comparisons of the MODIS  $T_b$  values to the calculated values include the noisy detectors in bands 21 and 22, the MODIS instrument NEDT, and the spatial variation in lake surface temperatures, which is larger in the small portion of Lake Titicaca. Sensitivity analysis shown in Table 3 indicates that the changes on the measured atmospheric temperature and water vapor profiles result in negligible or small effects on the calculated radiances in bands 20–23, 29, and 31–33. Therefore, it is useful to make comparisons in subareas of  $10 \times 16$  pixels where there was no in situ measurement but MODIS brightness temperatures in band 31 vary within a few tenths degree Kelvin by using the validated band 31 to determine lake surface temperatures. We found such subareas in the large portion of Lake Titicaca in cases of May 29 and June 13 and 15. The brightness temperatures in band 31 vary within  $\pm 0.13$ ,  $0.11$ , and  $0.07$  K in these subareas, respectively. The comparison results are given in Table 6. The values in columns 2–4 are copied from Table 4, while the values of the  $T_b$  difference in columns 5–7 are calculated from these three subareas. Note that no value is given in band 33 for the May 29 case in order to avoid the effect of a possible large temporal variation in the atmospheric temperature and water vapor profile because no profile was measured on May 29. If we use these  $T_b$  difference values as estimated calibration bias ( $\delta T_b$ ) in MODIS TIR bands, Fig. 9 shows the  $\delta T_b$  values in the six cases of daytime observations in Table 6 and the

nighttime case of June 23 (Table 5 column 13). Because atmospheric profiles were measured by radiosonde balloons on June 13 and 15, we should place more weights on the two cases in subareas of  $10 \times 16$  pixels in these 2 days. From these two cases, the averaged  $\delta T_b$  value is  $0.12$  and  $-0.19$  K in bands 31 and 32. It ranges from  $0.4$  to  $0.6$  K in bands 20–23, representing a calibration bias of 2–3% in the MODIS radiances according to Table 3 column 12.

We noticed that the averaged focal plane temperature was higher than the normal operational value by  $0.35$ – $0.60$  K in the short-wave and mid-wave IR (SW/MWIR) focal plane and by  $0.07$ – $0.32$  K in the long-wave (LWIR) focal plane in the period of our field campaign. The effect of changes in the averaged focal plane temperature was considered in the MODIS TIR calibration procedure. Any error in the coefficient for the effect of averaged focal plane temperature changes would result in a residual error in the calibration procedure. In order to estimate this residual error, we compared two nighttime cases through the same approach with the atmospheric temperature and water vapor profile measured on June 15, one on May 24 before the field campaign, another on June 23 after the field campaign. In the nighttime case of May 24, the average focal plane temperature was at the normal operational value,  $83.02$  K, in the LWIR focal plane and slightly higher than the normal operational value by  $0.27$  K in the SW/MWIR focal plane. From May 24 to June 23, the averaged focal plane temperature at the time of MODIS nighttime overpass changed by  $0.51$  and  $0.47$  K in the SW/MWIR and LWIR focal planes, respectively. The differences in the estimated calibration bias in bands 20, 29, and 31–32 between these two cases are less than  $0.1$  K. Therefore, we cannot simply attribute the calibration bias to the change of focal plane temperatures. However, the effect of changes in focal plane temperatures on the calibration of MODIS TIR bands needs further investigations.

The MODIS sensor was reconfigured on October 31 and November 1 to the B-side Science Mode from the A-side Science Mode [see Terra (PFM) Instrument Status and Terra MODIS History on webpage <http://mcstweb.gsfc.nasa.gov/Home.html>]. It appears that optical cross-talk from bands 31 to 32–36 is reduced by a significant amount, and cross-talk amongst bands 5–7 and 20–26 is also significantly reduced by transition to latest focal plane bias voltage (see Level-1B Code and Product Information on webpage <http://mcstweb.gsfc.nasa.gov/Home.html> and Bruce Guenther, 2001, personal communication). Vicarious calibration field campaigns are needed to provide quantitative estimates of these improvements and to evaluate the consistency (at different viewing angles and in different scenes) and stability (over a long period of time) of the radiometric accuracy of the MODIS TIR channels. Once the Aqua (EOS-PM-1) satellite is launched in the near future, the calibration accuracies of MODIS instruments aboard both Terra and Aqua platforms as well as the Atmospheric IR Sounder (AIRS) on the Aqua platform will be evaluated

with in situ measurement data from vicarious calibration field campaigns.

## 5. Error analysis

The error sources in the estimated calibration bias ( $\delta T_b$ ) include the effects of uncertainties in measured lake surface kinetic temperature and atmospheric conditions on the TOA radiance or equivalent brightness temperature values calculated by RTMs based on the measured lake surface temperature and atmospheric temperature and water profiles, noise and spatial variation in the MODIS data. The root sum squares (RSS) of uncertainties in the calibration accuracy estimate can be expressed as

$$\begin{aligned} \sigma^2 T_b = & \sigma^2 T_b(T_s) + \sigma^2 T_b(T_a) + \sigma^2 T_b(\text{wv}) \\ & + \sigma^2 T_b(\text{CO}_2) + \sigma^2 T_b(\text{O}_3) + \sigma^2 T_b(\text{RTM}) \\ & + \sigma^2 T_b(\text{NEDT} + S) \end{aligned} \quad (9)$$

where we use  $\sigma T_b(T_s)$  for the band brightness temperature uncertainty due to the uncertainty in the measured surface kinetic temperature, next four terms for the uncertainties in the atmospheric conditions,  $\sigma T_b(\text{RTM})$  for the uncertainty due to the atmospheric RTM MODTRAN4.0, and  $\sigma T_b(\text{NEDT} + S)$  for the uncertainties due to instrument noise and spatial variation in MODIS data.

We made a detailed error analysis of the measured lake surface kinetic temperature. The accuracy of the IR radiometers is better than 0.2 K (details given in Section 3). As shown in Fig. 7, the spatial pattern in the lake surface kinetic temperature measured by the five IR radiometers at the night and day times of Terra overpass is consistent with the spatial pattern in the  $T_b$  values from the MODIS L1B data. At the nighttime overpass, the average and standard deviation of the measured lake surface temperature are 284.18 and 0.35 K, respectively. They are 284.97 and 0.29 K at the daytime overpass. Dividing the standard deviation by square

root of 5, we got 0.16 K for the uncertainty in the averaged lake surface kinetic temperature at the nighttime overpass and 0.13 K at the daytime overpass. The 0.7-K temperature correction for lake surface emissivity depends on the RSR function of the IR radiometer (Fig. 4). We do not know the measured uncertainty in the RSR. If the first peak or the third peak in the RSR is reduced by 10%, the 0.7-K temperature correction term will change by  $\pm 0.06$  K. If both the first and third peaks are reduced by 10%, a resulting change in the 0.7-K temperature correction term will be negligible. The RSS of the instrument error in IR radiometer data, the uncertainty of 0.06 K in the temperature correction term, and the uncertainty due to spatial variations in lake surface kinetic temperatures is 0.26 K for both the daytime and nighttime cases. The effect of the RSS uncertainty 0.26 K on  $\sigma T_b(T_s)$  is given in Table 7 column 2.

Considering the instrument noise of radiosonde sensors and the temporal–spatial variations, we used 1.5 K and 15% as conservative estimates of uncertainties in atmospheric temperature and water vapor profiles. Note that we can also consider the 15% as the uncertainty in the absorption coefficients of atmospheric water vapor. We used 2 ppm, an estimated range of the seasonal cycle in  $\text{CO}_2$  mixing ratio, since we did not measure it in the field. An uncertainty of 6% in atmospheric ozone profile is also just an estimate since there is no direct measurement of ozone distribution in the MODIS viewing direction. By scaling the values in Table 3, we got the values in Table 7 columns 3–6 for the effects of uncertainties in atmospheric conditions.

The uncertainty in the TOA brightness temperature values in MODIS TIR bands calculated by the MODTRAN4.0 code for the measured surface and atmospheric conditions depends on the validated accuracy of the atmospheric radiative transfer code through comparisons with the line-by-line RTM in clear-sky conditions. A validated correlative- $k$  model (Mlawer, Taubman, Brown, Iacono, & Clough, 1997) is used in the MODTRAN4.0 code. Extensive atmospheric spectral radiance measurements have been made with the AERI (Revercomb et al., 1993) in various

Table 7

The RSS of uncertainties in the calibration accuracy estimate of MODIS TIR bands in this study

Band no.	$\sigma T_b(T_s)$ (0.26 K)	$\sigma T_b(T_a)$ (1.5 K)	$\sigma T_b(\text{wv})$ (15%)	$\sigma T_b(\text{CO}_2)$ (2 ppm)	$\sigma T_b(\text{O}_3)$ (6%)	$\sigma T_b(\text{RTM})$ (K)	$\sigma T_b(\text{NEDT})$ (K)	RSS $\sigma T_b$ (K)	RSS $\sigma L/L$ (%)
20	0.24	0.06	0.03			0.07	0.06	0.27	1.2
11	0.25	0.06				0.06	0.64	0.69	3.1
12	0.25	0.06				0.06	0.07	0.27	1.2
13	0.24	0.12				0.12	0.05	0.30	1.3
9	0.24	0.12	0.08		0.01	0.14	0.03	0.31	0.7
1	0.25	0.06	0.05			0.08	0.03	0.28	0.4
32	0.25	0.06	0.06			0.08	0.05	0.28	0.4
33	0.16	0.51	0.06	0.04	0.04	0.52	0.16	0.77	1.1
24	0.08	0.78		0.02		0.78	0.13	1.11	5.6
25	0.16	0.48	0.02		0.01	0.48	0.08	0.70	3.1
30	0.17	0.54	0.02		0.55	0.77	0.08	1.10	2.3
34	0.07	0.81	0.03	0.06	0.03	0.81	0.27	1.18	1.9
35	0.04	0.99	0.02	0.05	0.04	0.99	0.23	1.42	2.5
36	0.01	1.20	0.02	0.05		1.20	0.41	1.75	3.3

sites of the Atmospheric Radiation Measurement (ARM) program (Stokes & Schwartz, 1994). The validation activities for the line-by-line RTM model indicate that the limiting error in these validations is due to the specification of the water vapor profile (Mlawer et al., 1997) and that the major contributions to the error are the uncertainties in the temperature and water vapor profiles (Walden, Warren, & Murcray, 1998). These conclusions indicate that  $\sigma T_b(\text{RTM})$  should be site dependent, i.e., the error in the atmospheric radiative transfer simulations would be smaller in high-altitude sites in dry seasons. Therefore, we used the RSS of values in Table 7 columns 3–6 as the estimate of  $\sigma T_b(\text{RTM})$  in column 7. In this way, the effects of the uncertainties in atmospheric conditions are considered twice in Eq. (9). We think that this represents the worst scenario. In other words, the actual  $\sigma T_b(\text{RTM})$  value may be smaller.

The  $\sigma T_b(\text{NEDT})$  values in column 8 are copied from Table 3 column 9 that were estimated from real MODIS data (Wan, in press). Based on the values in columns 2–8, Eq. (9) gives  $\sigma T_b$  values in column 9 and corresponding relative radiance errors in column 10.

In the point comparison between MODIS data and the TOA brightness temperatures calculated from the measured atmospheric profiles and lake surface kinetic temperatures in the small portion of Lake Titicaca by the Village of Huatajata, we need to consider the uncertainty due to noise and the spatial variation in MODIS data. The actual NEDT in a single MODIS pixel may be two to three times the standard deviation value listed in Table 7 and could be up to five times the value in worst cases. Therefore, it is reasonable to assume a NEDT value of 0.1–0.2 K for bands 20, 22–23, 29, and 31–32, even a larger value for other bands. However, the effect of NEDT is much smaller in the cases of subareas of  $10 \times 16$  pixels (shown in column 13 of Table 5 and columns 5–7 in Table 6) because the MODIS  $T_b$  value was averaged over 160 pixels. Because there was no radiosonde balloon launched at these subareas, the effect of uncertainties in atmospheric conditions may be larger. However, these cases of subareas were selected only in calm clear-sky conditions. We expect that the difference in atmospheric conditions over the large and small portions of Lake Titicaca would be less than 1.5 K in temperature profile and 15% in the low portion of the water vapor profile. We confirmed this by comparing the values between columns 3 and 6 and between columns 4 and 7 in Table 6, their differences all being less than the values in Table 7 column 9. If the error in radiances calculated by the MODTRAN4.0 code in dry atmospheric conditions is much less than the values in column 7, we do not need to consider the effects of uncertainties in atmospheric conditions twice. Then, we can use the values in column 7 as RSS  $\sigma T_b$  because both the  $\sigma T_b(T_s)$  and  $\sigma T_b(\text{NEDT})$  are much smaller. This means that the actual RSS  $\sigma T_b$  may be smaller than the values in Table 7 column 9. According to the RSS  $\sigma T_b$  values in Table 7 column 9, the 14 MODIS TIR bands (excluding the water vapor sounding bands 27 and 28 that are too sensitive to the uncertainty in

measured water vapor profile) were listed in two groups. The first group includes six bands in the atmospheric windows (i.e., bands 20–23, 29, and 31–32) and band 33. The second group includes five atmospheric temperature sounding bands (i.e., bands 24–25 and 34–36) and the ozone band 30. We can see that in the first group the RSS  $\sigma T_b$  values are smaller or slightly larger than the  $\delta T_b$  values for the specified calibration accuracies given in Table 3 column 12. The corresponding RSS of errors in the calibration accuracy estimate is about 0.4% in bands 31 and 32, 0.7% in band 29, 3% in band 21, and slightly larger than 1% in bands 20, 22–23, and 33. However, the RSS  $\sigma T_b$  values in the second group are much larger than the values that are required to achieve the specified calibration accuracies. This means that the radiosondes cannot provide accurate atmospheric temperature and water vapor profiles to estimate the calibration accuracies in the atmospheric sounding bands (bands 24–25, 27–28, and 34–36) at the specified 1% level and that the calibration accuracy in the ozone band 30 cannot be estimated without in situ measurements of ozone. In order to estimate the calibration accuracy in these bands, it is necessary to launch multiple radiosondes at more than one sites and to measure the atmospheric radiation continuously at the direction toward the MODIS instrument during the overpass so that the temporal and spatial variations in atmospheric temperature and water vapor profiles can be analyzed to better estimate the actual uncertainties in the profiles.

As shown in Table 3, the difference of brightness temperatures in bands 31 and 32 is much less sensitive to the variations in atmospheric conditions because of the dry atmospheric condition. If we use the four cases of June 13 and 15 (columns 3–4 and 6–7 in Table 6) to estimate this difference, it is  $0.32 \pm 0.06$  K.

Because the polarization of thermal emittance from water surface is zero at nadir direction and it increases with viewing angle (Shaw, 1999), the calibration error caused by the unpolarized scene assumption in the MODIS L1B processing would also increase with viewing angle if it is a major error source. In the six daytime cases and one nighttime case shown in Fig. 9 (see Table 6 and column 13 in Table 5 for details), the MODIS Earth view zenith angle (defined at the surface) ranges from  $53.5^\circ$ ,  $49.8^\circ$ , and  $19.6^\circ$  before the Earth nadir view to  $27.6^\circ$ ,  $34.3^\circ$ ,  $48.1^\circ$ , and  $51.6^\circ$  after the Earth nadir view. We could not see obvious evidence of the viewing angle dependence in the  $\delta T_b$  values. Therefore, we could not make a quantitative estimate of the polarization-related calibration error. However, it appears that the  $\delta T_b$  values in these cases indicate that this polarization-related calibration errors is not larger than 0.2 K in bands 29 and 31–32. We also compared the MODIS TIR data over a subarea of  $10 \times 16$  pixels in the large portion of Lake Titicaca in the nighttime overpass on May 24 with the calculated TOA radiances based on the atmospheric temperature and water vapor profiles measured on June 15. In that granule (A2000145.0330), the viewing zenith angle was  $1.2^\circ$ . The  $\delta T_b$  values in bands 20, 29, and 31–32 agree with the values shown in Fig. 9 within

$\pm 0.1$  K, giving another evidence that the polarization-related calibration error is small.

We understand that it has been an ongoing research activity for a long time to accurately validate the absolute accuracy of atmospheric RTMs such as MODTRAN and line-by-line RTMs in the TIR region. As shown in the above error analysis, the effect of uncertainties in the accuracy of atmospheric RTMs on the estimate of calibration bias in the eight MODIS TIR bands is small when using high-elevation Lake Titicaca as a calibration site. Therefore, we can estimate a calibration bias of 2–3% in MODIS bands 20, 22 and 23, with a RSS uncertainty not larger than 1.3%, estimate the calibration accuracy in band 33 barely at the specification, and estimate calibration accuracies in other four bands better than the specifications.

## 6. Conclusion

The absolute radiometric accuracy of MODIS TIR channel data was evaluated with in situ measurement data collected in Lake Titicaca, Bolivia during May and June 2000. Sensitivity and error analysis was made to study the effects of uncertainties in measured surface temperatures and atmospheric profiles. The absolute radiometric accuracies specified for the MODIS bands above 3  $\mu\text{m}$  are achieved or nearly achieved in bands 21, 29, and 31–33. The radiometric calibration error is less than 0.4% in bands 31 and 32. The calibration error in the high-temperature band 21 for fire detection is less than 1 K at scene temperatures around 285 K in most cases. Comparisons indicate a calibration bias of 2–3% in bands 20, 22, and 23. The sensitivity study and error analysis show that the radiosondes cannot provide accurate atmospheric temperature and water vapor profiles to estimate the calibration accuracies in other bands at the specified 1% level. The relative calibration accuracy between the split-window bands 31 and 32 (i.e., the accuracy in the difference of brightness temperatures in these two bands) was estimated as  $0.32 \pm 0.06$  K, which is enough to make a significant impact on the MODIS SST retrieval and a moderate impact on the MODIS LST retrieval.

## Acknowledgments

This work was supported by EOS Program contract NAS5-31370 of the National Aeronautics and Space Administration. The authors would like to thank Dr. Xingfa Gu, INRA-Bioclimatology, France, Ms. Sophie Moreau, National Coordinator of Bolivia Association of Remote Sensing for the Environment (ABTEMA), Mr. Carlos Diaz, National Director of the National Service of Meteorology and Hydrology, Bolivia, and Dr. Bernard Pouyau, Director of the French Institute of Research for Development (IRD), Bolivia, for their help in the preparation and implementation of the field campaign conducted in Bolivia

in May/June 2000. The MODIS data were generated by the Goddard DAAC and MODAPS under the support of MODIS MCST and SDDT. We also used the EP/TOMS total ozone image of 15 June 2000 from the NASA TOMS webpage (<http://toms.gsfc.nasa.gov>). The authors would like to thank the three anonymous reviewers for their valuable detailed comments and suggestions, which helped to improve the paper.

## References

- Barnes, W. L., Pagano, T. S., & Salomonson, V. V. (1998). Prelaunch characteristics of the Moderate Resolution Imaging Spectroradiometer (MODIS) on EOS-AM1. *IEEE Transactions on Geoscience and Remote Sensing*, 36 (4), 1088–1100.
- Berk, A., Anderson, G. P., Bernstein, L. S., Acharya, P. K., Dothe, H., Matthew, M. W., Adler-Golden, S. M., Chetwynd Jr., J. H., Richtmeier, S. C., Pukall, B., Allred, C. L., Jeong, L. S., & Hoke, M. L. (1999). MODTRAN4 radiative transfer modeling for atmospheric correction. In: *Optical spectroscopic techniques and instrumentation for atmospheric and space research III, Proc. SPIE, Bellingham, Washington*. vol. 3756 (pp. 348–353).
- Boehm, M. T., & Verlinde, J. (2000). Stratospheric influence on upper tropospheric tropical cirrus. *Geophysical Research Letters*, 27 (19), 3209–3212.
- Born, M., & Wolfe, E. (1980). *Principles of optics* (6th ed.). New York: Pergamon.
- Bruegge, C. J., Conel, J. E., Green, R. O., Margolis, J. S., Holm, R. G., & Toon, G. (1992). Water vapor column abundance retrievals during FIFE. *Journal of Geophysical Research*, 97 (D17), 18759–18768.
- Chesters, D., & Neuendorffer, A. (1991). Comparison between TOMS, TOVS and DOBSON observations: satellite and surface views of total column ozone. *Global and Planetary Changes*, 90, 61–67.
- Clough, S. E., Kneizys, F. X., Shettle, E. P., & Anderson, G. P. (1986). Atmospheric radiance and transmission: FASCOD2. In: *Proc. of the sixth conference on atmospheric radiation, Williamsburg, VA* (pp. 141–144). Boston, MA: American Meteorological Society.
- Esaias, W. E., Abbott, M. R., Barton, I., Brown, O. W., Campbell, J. W., Carder, K. L., Clark, D. K., Evans, R. L., Hoge, F. E., Gordon, H. R., Balch, W. P., Letelier, R., & Minnett, P. J. (1998). An overview of MODIS capabilities for ocean science observations. *IEEE Transactions on Geoscience and Remote Sensing*, 36 (4), 1250–1265.
- Guenther, B., Godden, G. D., Xiong, X., Knight, E. J., Qiu, S.-Y., Montgomery, H., Hopkins, M. M., Khayat, M. G., & Hao, Z. (1998). Prelaunch algorithm and data format for the level 1 calibration product for the EOS-AM1 Moderate Resolution Imaging Spectroradiometer (MODIS). *IEEE Transactions on Geoscience and Remote Sensing*, 36 (4), 1142–1151.
- Hale, G. M., & Query, M. R. (1973). Optical constants of water in the 200-nm to 200- $\mu\text{m}$  wavelength region. *Applied Optics*, 12 (3), 555–641.
- Justice, C. O., Vermote, E., Townshend, J. R. G., Defries, R., Roy, D. O., Hall, D. K., Salomonson, V. V., Privette, J. L., Riggs, G., Strahler, A., Lucht, W., Myneni, R. B., Knyazikhin, K., Running, S. W., Nemani, P. R., Wan, Z., Huete, A. R., van Leeuwen, W., Wolfe, R. E., Giglio, L., Muller, J.-P., Knyazikhin, Y., & Barnsley, M. J. (1998). The Moderate Resolution Imaging Spectroradiometer (MODIS): land remote sensing for global change research. *IEEE Transactions on Geoscience and Remote Sensing*, 36, 1228–1249.
- King, M. D., Herring, D. D., & Diner, D. J. (1995). The Earth Observing System (EOS): a space-based program for assessing mankind's impact on the global environment. *Optical Photometry News*, 6, 34–39.
- King, M. D., Kaufman, Y. J., Menzel, W. P., & Tanré, D. (1992). Remote sensing of cloud, aerosol, and water vapor properties from the Moderate

- Resolution Imaging Spectrometer (MODIS). *IEEE Transactions on Geoscience and Remote Sensing*, 30 (1), 2–27.
- King, M. D., Menzel, W. P., Grant, P. S., Myers, J. S., Arnold, G. T., Platnick, S. E., Gumley, L. E., Tsay, S. C., Moeller, C. C., Fitzgerald, M., Brown, K. S., & Osterwisch, F. G. (1996). Airborne scanning spectrometer for remote sensing of cloud, aerosol, water vapor and surface properties. *Journal of Atmospheric and Oceanic Technology*, 13, 777–794.
- Masuda, K., Takashima, T., & Yakayma, Y. (1988). Emissivity of pure and sea waters for the model sea surface in the infrared window regions. *Remote Sensing of Environment*, 24, 313–329.
- McFarquhar, G. M., Heymsfield, A. J., Spenhirne, J., & Hart, B. (2000). Thin and subvisual tropopause tropical cirrus: observation and radiative impacts. *Journal of Atmospheric Science*, 29 (20), 1841–1853.
- Miloshevich, L. M., Vömel, H., Paukkn, A., Heymsfield, A. J., & Oltmans, S. J. (2001). Characterization and correction of relative humidity measurements from Vaisala RS80-A radiosondes at cold temperatures. *Journal of Atmospheric and Oceanic Technology*, 18, 135–156.
- Mlawer, E. J., Taubman, S. J., Brown, P. D., Iacono, M. J., & Clough, S. A. (1997). Radiative transfer for inhomogeneous atmospheres: RRTM, a validated correlated-k model for the longwave. *Journal of Geophysical Research*, 102 (D14), 16663–16682.
- Padilla, H. G., Leyva, A. C., & Mosino, P. A. (1993). An analysis of daily humidity patterns at a mountainous and urban site in a tropical high-altitude region. *Journal of Applied Meteorology*, 32, 1638–1646.
- Revercomb, H. E., Best, F. A., Dedecker, R. G., Dirks, T. P., Herbsleb, R. A., Knuteson, R. O., Short, J. F., & Smith, W. L. (1993). Atmospheric emitted radiance interferometer (AERI) for ARM. In: *Fourth symposium on global change studies*, Am. Meteorol. Soc., Boston, Mass. (pp. 46–49).
- Salomonson, V., Barnes, W., Maymon, P., Montgomery, H., & Ostrow, H. (1989). MODIS: advanced facility instrument for studies of the Earth as a system. *IEEE Transactions on Geoscience and Remote Sensing*, 27 (2), 145–153.
- Shaw, J. A. (1999). Degree of linear polarization in spectral radiances from water-viewing infrared radiometers. *Applied Optics*, 38 (15), 3157–3165.
- Smith, W. L., Knuteson, R. O., Revercomb, H. E., Feltz, W., Howell, H. B., Menzel, W. P., Nalli, N. R., Brown, O., Brown, J., Minnett, P., & Mckeown, W. (1996). Observations of the infrared radiative properties of the ocean — implications for the measurement of sea surface temperature via satellite remote sensing. *Bulletin of the American Meteorological Society*, 77 (1), 41–51.
- Snyder, W., Wan, Z., Zhang, Y., & Feng, Y.-Z. (1997). Requirements for satellite land surface temperature validation using a silt playa. *Remote Sensing of Environment*, 61 (2), 279–289.
- Starr, D. O., & Cox, S. K. (1985). Cirrus clouds: part II. Numerical experiments on the formation and maintenance of cirrus. *Journal of Atmospheric Science*, 42 (23), 2682–2694.
- Stokes, G. M., & Schwartz, S. E. (1994). The Atmospheric Radiation Measurement (ARM) program: programmatic background and design of the Cloud and Radiation Test Bed. *Bulletin of the American Meteorological Society*, 75, 1201–1221.
- Walden, V. P., Warren, S. G., & Murcray, F. J. (1998). Measurements of the downward longwave radiation spectrum over the Antarctic Plateau and comparisons with a line-by-line radiative transfer model for clear skies. *Journal of Geophysical Research*, 103 (D4), 3825–3846.
- Wan, Z. (2002). Estimate of noise and systematic error in early thermal infrared data of the Moderate Resolution Imaging Spectroradiometer (MODIS). *Remote Sensing of Environment*, 80 (1), 47–54.
- Wan, Z., & Dozier, J. (1996). A generalized split-window algorithm for retrieving land-surface temperature from space. *IEEE Transactions on Geoscience and Remote Sensing*, 34 (4), 892–905.
- Wan, Z., & Li, Z.-L. (1997). A physics-based algorithm for retrieving land-surface emissivity and temperature from EOS/MODIS data. *IEEE Transactions on Geoscience and Remote Sensing*, 35 (4), 980–996.
- Wan, Z., Zhang, Y., Ma, X., King, M. D., Myers, J. S., & Li, X. (1999). Vicarious calibration of the Moderate-Resolution Imaging Spectroradiometer Airborne Simulator thermal infrared channels. *Applied Optics*, 38 (20), 6294–6306.